JCI The Journal of Clinical Investigation

Protein kinase N1 critically regulates cerebellar development and longterm function

Stephanie zur Nedden, … , Gottfried Baier, Gabriele Baier-Bitterlich

J Clin Invest. 2018. https://doi.org/10.1172/JCI96165.

Research Article In-Press Preview **Neuroscience**

Increasing evidence suggests that synapse dysfunctions are a major determinant of several neurodevelopmental and neurodegenerative diseases. Here we identify protein kinase N1 (PKN1) as a novel key player in fine-tuning the balance between axonal outgrowth and presynaptic differentiation in the parallel fiber (PF)-forming cerebellar granule cells (Cgc). Postnatal *Pkn1*$^{-/-}$ animals showed a defective PF-Purkinje cell (PC) synapse formation. In vitro, *Pkn1*$^{-/-}$ Cgc exhibited deregulated axonal outgrowth, elevated AKT phosphorylation and higher levels of neuronal differentiation-2 (NeuroD2), a transcription factor preventing presynaptic maturation. Concomitantly *Pkn1*$^{-/-}$ Cgc had a reduced density of presynaptic sites. By inhibiting AKT with MK-2206 and siRNA-mediated knockdown, we found that AKT hyperactivation is responsible for the elongated axons, higher NeuroD2 levels and the reduced density of presynaptic specifications in *Pkn1*$^{-/-}$ Cgc. In line with our in vitro data, *Pkn1*$^{-/-}$ mice showed AKT hyperactivation, elevated NeuroD2 levels and reduced expression of PF-PC synaptic markers during stages of PF maturation in vivo. The long-term effect of *Pkn1* knockout was further seen in cerebellar atrophy and mild ataxia. In summary, our results demonstrate that PKN1 functions as a developmentally active gatekeeper of AKT activity, thereby fine-tuning axonal outgrowth and presynaptic differentiation of Cgc and subsequently the correct PF-PC synapse formation.

Research Article

Protein kinase N1 critically regulates cerebellar development and longterm function

Stephanie zur Nedden,[1] Rafaela Eith,[1] Christoph Schwarzer,[2] Lucia Zanetti,[3] Hartwig Seitter,[3] Friedrich Fresser,[4] Alexandra Koschak,[3] Angus J.M. Cameron,[5] Peter J. Parker,[6] Gottfried Baier,[4] and Gabriele Baier-Bitterlich[1]

[1]Medical University of Innsbruck, Biocenter, Division of Neurobiochemistry, Innrain 80-82, 6020 Innsbruck, Austria.

[2]Medical University of Innsbruck, Department of Pharmacology, Peter Mayr Strasse 1a, 6020 Innsbruck, Austria.

[3]University of Innsbruck, Institute of Pharmacy, Pharmacology and Toxicology, Center for Molecular Biosciences, Innrain 80-82, 6020 Innsbruck, Austria.

[4]Medical University of Innsbruck, Department for Pharmacology and Genetics, Division of Translational Cell Genetics, Peter Mayr Strasse 1a, 6020 Innsbruck, Austria.

[5]Kinase Biology Laboratory, John Vane Science Centre, Barts Cancer Institute, Queen Mary University of London, Charterhouse Square, London EC1M 6BQ, UK.

[6]Francis Crick Institute, Midland Road, London NW1 1AT, UK and the Division of Cancer Studies, King's College London, New Hunt's House, St Thomas Street, London SE1 1UL, UK.

Address correspondence to**:** Gabriele Baier-Bitterlich, Medical University of Innsbruck, Biocenter, Division of Neurobiochemistry, Innrain 80-82, 6020 Innsbruck, Austria. Phone: 43.512.9003.70289; Email: gabriele.baier-bitterlich@i-med.ac.at;

ORCID 0000-0002-7009-8168

Conflict of interest statement: The authors have declared that no conflict of interest exists.

Abstract

Increasing evidence suggests that synapse dysfunctions are a major determinant of several neurodevelopmental and neurodegenerative diseases. Here we identify protein kinase N1 (PKN1) as a novel key player in fine-tuning the balance between axonal outgrowth and presynaptic differentiation in the parallel fiber (PF)-forming cerebellar granule cells (Cgc). Postnatal *Pkn1*$^{-/-}$ animals showed a defective PF-Purkinje cell (PC) synapse formation. In vitro, *Pkn1*$^{-/-}$ Cgc exhibited deregulated axonal outgrowth, elevated AKT phosphorylation and higher levels of neuronal differentiation-2 (NeuroD2), a transcription factor preventing presynaptic maturation. Concomitantly *Pkn1*$^{-/-}$ Cgc had a reduced density of presynaptic sites. By inhibiting AKT with MK-2206 and siRNA-mediated knockdown, we found that AKT hyperactivation is responsible for the elongated axons, higher NeuroD2 levels and the reduced density of presynaptic specifications in *Pkn1*$^{-/-}$ Cgc. In line with our in vitro data, *Pkn1*$^{-/-}$ mice showed AKT hyperactivation, elevated NeuroD2 levels and reduced expression of PF-PC synaptic markers during stages of PF maturation in vivo. The long-term effect of *Pkn1* knockout was further seen in cerebellar atrophy and mild ataxia. In summary, our results demonstrate that PKN1 functions as a developmentally active gatekeeper of AKT activity, thereby fine-tuning axonal outgrowth and presynaptic differentiation of Cgc and subsequently the correct PF-PC synapse formation.

Introduction

Protein kinase N1 (PKN1/ PRK1) is the most abundantly expressed isoform of the PKN family in the central nervous system and accounts for 0.01% of total brain protein (1). It is widely studied for its involvement in cancer (2), however surprisingly little is known about the brain-specific function of this kinase, even though it was first isolated from human hippocampal cDNA in 1994 (3) and is particularly enriched in certain brain areas (4). In human neurons PKN is mainly localized to juxtanuclear, cytoplasmic, dendroplasmic, pre- and postsynaptic compartments (5).

PKN1 is a serine/threonine kinase and belongs to the protein kinase C superfamily, sharing a characteristic C-terminal catalytic domain (3, 6) that requires phosphorylation by PDK-1 for activation. The N-terminal regulatory domain confers binding and regulation by RhoA/B/C, Rac1 (7), fatty acids and phospholipids (8). Activation of PKN1 is also achieved by caspase-3-mediated cleavage, resulting in a constitutively active protein product missing the regulatory N-terminus (9). This form of deregulated PKN1 activation occurs during apoptosis (10) and has been linked to various insults to the brain (11-14). We have previously reported that PKN1 is part of a purine-nucleoside signaling cascade involved in the protection of hypoxic neuronal cultures and cell lines in vitro (15, 16). However, despite those in vitro reports and evidence on the generation of a constitutively active fragment, the physiological function of PKN1 in the nervous system in vivo is not yet known.

Using *Pkn1*$^{-/-}$ animals (17) this work set out to clarify the role of PKN1 in the brain. We focused on the cerebellum, which has a central role in motor control and coordination and is also the brain area with the highest PKN1 expression levels (4). The lengthy process to achieve cerebellar maturity makes it particularly susceptible to developmental abnormalities, which may finally result in neurodegeneration and disabilities such as cerebellar ataxia (18). Two excitatory afferents converge onto Purkinje cells (PC), the only output neurons of the cerebellum: climbing fibers (CF) from inferior olivary nuclei and parallel fibers (PF) from cerebellar granule cells (Cgc). A hallmark in cerebellar development is the correct formation of the PF-PC synapse (19), which is important for the segregation of CF and PF territories (20, 21) and cerebellar long term function (22). PF-PC synaptic dysfunctions have been implicated in models of spinocerebellar ataxias 1, 3, 5 and 27, Friedreich's ataxia as well as autism spectrum disorders (19, 23). Considering the high expression levels of PKN1 in Cgc and PC (4), we investigated the effect of *Pkn1* deletion on the formation of PF-PC as well as CF-PC synapses during cerebellar development.

Our results demonstrate that during cerebellar development PKN1 functions as a gatekeeper of AKT activity and subsequently protein levels of the transcription factor neuronal differentiation 2 (NeuroD2), thereby fine-tuning axonal outgrowth and presynaptic differentiation of Cgc. Accordingly, *Pkn1* deletion results in disrupted PF-PC synapse formation and defective CF elimination, as seen in a reduced expression of the PF-PC synaptic marker cerebellin1 (Cbln1), persistent multiple CF innervation and reduced spontaneous PC activity. The long-term effect of *Pkn1* deletion was further seen in cerebellar atrophy and mild ataxia in adult *Pkn1*$^{-/-}$ animals. Despite the rapidly increasing literature on AKT signaling and neurodevelopment, this is, to our knowledge, the first report linking developmental AKT activity with NeuroD2 levels and cerebellar synapse formation, and we identify PKN1 as a regulator of this pathway.

Results

Deletion of Pkn1 leads to a defective parallel fiber-Purkinje cell synapse formation and Purkinje cell activity. We first analyzed CF growth, as an indicator of a functioning PF-PC synapse formation, by staining of cerebellar sections of postnatal day (P) 8-P15 WT and *Pkn1*$^{-/-}$ animals with the CF-specific marker vesicular glutamate transporter 2 (VGlut2) (20). Early during cerebellar development PC somata are innervated by multiple CF. From P9 onwards a single "winner" CF starts dendritic translocation and expands its territory (20). Perisomatic CF synapse elimination occurs in an early, PF-independent phase (~P7–11), and a late phase (~P12–17), which, similar to the proximal dendritic restriction of CF innervation, strictly depends on a functioning PF-PC synapse (21). There were no differences between WT and *Pkn1*$^{-/-}$ animals in VGlut2-stained CF terminals at P8, where they were mainly found around the PC somata (Figure 1, A and B). However, as compared to WT animals, cerebella of P15 *Pkn1*$^{-/-}$ mice showed an enhanced distal extension of CF terminals into PF territory (Figure 1, A and B) and a defective perisomatic CF elimination (Figure 1, A and C). Western blot analysis further revealed that the ratio of VGlut2 to the PF-specific marker vesicular glutamate transporter 1 (VGlut1) (20) dropped from P8 to P15 in WT animals but stayed the same in *Pkn1*$^{-/-}$ animals (Supplemental Figure 1A), further showing imbalances in CF/PF innervation. VGlut1 expression was consistently lower in *Pkn1*$^{-/-}$ animals during development (Supplemental Figure 1A). Starting at P15, we detected dendritic thickening of *Pkn1*$^{-/-}$ PC that coincided with the defective CF growth (Supplemental Figure 1B). At these early developmental stages, those defects did not translate into altered cerebellar morphology of *Pkn1*$^{-/-}$ mice. WT and *Pkn1*$^{-/-}$ mice showed a similar cerebellar size, foliation pattern and thickness of the external granule layer (EGL), internal granule layer (IGL) and molecular layer (ML) (Supplemental Figure 1C).

To reveal potential CF synapse elimination deficits in *Pkn1*$^{-/-}$ animals we measured CF-induced excitatory postsynaptic currents (ePSC) in PC in acute slices prepared from P15-17 old animals (24). With gradually increasing stimulus intensities, the majority of ePSCs of WT PC were obtained in an all-or-none fashion, while the majority of ePSCs of *Pkn1*$^{-/-}$ PC occurred at two or more discrete steps (Figure 1D). This indicates a more frequent occurrence of multiple CF innervation in *Pkn1*$^{-/-}$ mice.

To further expose a functional defect in PF-PC synapse formation we recorded spontaneous ePSCs of PC in acute slices prepared from P13-P15 old WT and *Pkn1*$^{-/-}$ animals. Recordings were performed at room temperature to avoid intrinsic PC firing (25) and therefore ePSCs mainly reflect PF synapse activity (26, 27). Interestingly *Pkn1*$^{-/-}$ PC showed reduced ePSC frequencies (Figure 1E) but similar ePSC amplitudes (Supplemental Figure 1D), indicating differences in the number of functional synapses but not in presynaptic quantal content or postsynaptic receptors. Likewise, *Pkn1*$^{-/-}$ cerebellar slices had a reduced inhibitory (i) PSC input (Supplemental Figure 1E), which might also be caused by a defective PF-ML interneuron synapse formation.

We next tested the expression of the PF-PC synaptic markers cerebellin 1 (Cbln1), a protein excreted by Cgc and important for PF-PC synapse stabilization (22, 28), as well as δ2 glutamate receptor (GluD2), the PC postsynaptic receptor binding to extracellular Cbln1 (29). Consistently with a defective PF-PC synapse formation, Cbln1 expression levels were lower in P15 *Pkn1*$^{-/-}$ cerebella (Figure 1, F and G). GluD2 expression levels were however only marginally affected (Figure 1, F and H), suggesting a Cgc-specific defect. We next screened in vitro Cgc for differences in presynaptic maturation and axonal outgrowth properties, since the correct balance between axonal growth and presynaptic differentiation is an essential part of synapse formation (30).

PKN1 regulates axonal outgrowth and the density of presynaptic sites in Cgc in vitro. We first analyzed mature Cgc cultures (4-7 days in vitro, DIV) for differences in presynaptic sites, which appear as 'en passant swellings' (31) along the axon. These varicosities show colocalization of TAU and the presynaptic marker Synapsin I (Figure 2A). In *Pkn1*$^{-/-}$ Cgc transfected with HA-tagged human *PKN1* (h*PKN1*), HA-staining was found around the nucleus, in dendrites and along those en passant swellings of the axon (Supplemental Figure 2, A and B). Interestingly mature *Pkn1*$^{-/-}$ Cgc cultures had a reduced density of presynaptic sites (Figure 2B), an effect that could be rescued by reintroduction of h*PKN1* (Figure 2C). *Pkn1* knockout also resulted in deregulated axonal outgrowth, as seen in elongated axons of *Pkn1*$^{-/-}$ Cgc throughout the entire culture period (Figure 2D). The enhanced axonal outgrowth was reduced to WT levels in *Pkn1*$^{-/-}$ Cgc transfected with h*PKN1* (Figure 2E). These results point towards elongated axonal outgrowth at the expense of presynaptic differentiation in *Pkn1*$^{-/-}$ Cgc. We therefore next screened Cgc protein extracts for differences in PKN1 downstream signaling molecules involved in presynaptic differentiation and axonal outgrowth.

Pkn1 knockout results in enhanced AKT phosphorylation and NeuroD2 expression in Cgc in vitro. An important regulator of axonal outgrowth is the protein kinase AKT (32) and PKN1 has been previously suggested to negatively regulate AKT activity (33), for example downstream of the B-cell antigen receptor (34). We found that Cgc from *Pkn1*$^{-/-}$ mice showed significantly higher endogenous AKT phosphorylation levels at T308 and S473 (Supplemental Figure 2C). The mean pAKT T308 (Figure 3A) and pAKT S473 (Supplemental Figure 2D) intensity of *Pkn1*$^{-/-}$ Cgc was consistently reduced in h*PKN1*-transfected cells, but not in *GFP*-transfected cells (Supplemental Figure 2E), showing that the higher AKT phosphorylation was specifically caused by the absence of PKN1. We next tested if *Pkn1* knockout-mediated AKT hyperactivation is the cause of elongated axonal outgrowth, by incubating Cgc with the potent

AKT inhibitor MK-2206 (Supplemental Figure 3A). MK-2206 reduced the axonal length of *Pkn1*$^{-/-}$ Cgc to WT levels (Figure 3B), establishing PKN1 as a regulator of axonal length upstream of AKT.

Interestingly we found that mature *Pkn1*$^{-/-}$ Cgc cultures had higher NeuroD2 protein levels (Figure 3C). Transfection of *Pkn1*$^{-/-}$ Cgc with h*PKN1*, but not with *GFP* (Supplemental Figure 3B), reduced the mean NeuroD2 intensity in immunofluorescence stainings (Figure 3D), establishing PKN1 as a negative regulator of NeuroD2 levels. This fits well with our observation of a defective spacing of presynaptic sites in *Pkn1*$^{-/-}$ Cgc (Figure 2B), since NeuroD2 is a transcription factor preventing presynaptic differentiation, whose overexpression reduces the density of presynaptic sites in Cgc (30). Since AKT has been shown to enhance the activity of several transcription factors regulating NeuroD2 expression, such as neurogenin1 and neuronal differentiation 1 (NeuroD1) (35, 36), we next tested if AKT regulates NeuroD2 protein levels in Cgc.

In protein extracts of WT Cgc at DIV1 treated with MK-2206 for 24 h, we found that MK-2206 dose-dependently reduced NeuroD2 levels (Figure 3E). Additionally, we detected enhanced Cbln1 expression upon inhibition of AKT (Supplemental Figure 3C). MK-2206 had similar effects in *Pkn1*$^{-/-}$ Cgc (Supplemental Figure 3D). Furthermore, *Pkn1*$^{-/-}$ Cgc showed a trend towards reduced Cbln1 levels (Supplemental Figure 3E). To further validate those results we next suppressed AKT expression in order to see if the observed phenotype of *Pkn1*$^{-/-}$ Cgc could be restored to WT levels.

siRNA-mediated knockdown of Akt123 restores axonal length, NeuroD2 expression levels and the density of presynaptic sites in Pkn1$^{-/-}$ *Cgc to WT levels.* WT and *Pkn1*$^{-/-}$ Cgc were transfected with siRNAs targeting *Akt123* or control non-targeting siRNAs and stained for pan-AKT.

Akt123 siRNAs significantly reduced pan-AKT expression at DIV1 and DIV4 (Figure 4A and Supplemental Figure 4, A and B). The concentration of *Akt* siRNAs was chosen to accomplish a significant decrease in AKT without adverse effect on cell viability. Knockdown of *Akt123* significantly reduced the enhanced axonal length of *Pkn1*$^{-/-}$ Cgc at DIV1 (Figure 4B). Similarly, elevated NeuroD2 levels in *Pkn1*$^{-/-}$ Cgc were restored to WT levels upon *Akt123* knockdown (Figure 4C) and accompanied by an increased density of presynaptic sites (Figure 4D). Knockdown of *Akt123* also resulted in an enhanced expression of Cbln1 in WT (Supplemental Figure 4C) and *Pkn1*$^{-/-}$ Cgc (Supplemental Figure 4D). These data confirm our previous findings that PKN1-mediated modulation of AKT is crucial for the balance between axonal outgrowth, NeuroD2/Cbln1 expression and presynaptic differentiation. We therefore next tested AKT phosphorylation and NeuroD2 expression during in vivo development in WT and *Pkn1*$^{-/-}$ animals.

Cerebellar alterations in Pkn1$^{-/-}$ *mice coincide with developmentally enhanced AKT phosphorylation and NeuroD2 expression in vivo.* Protein lysates prepared from P1-P15 WT cerebella showed an inverse correlation between PKN1 expression dropping and AKT phosphorylation increasing during development (Figure 5A). Concomitantly we found higher AKT phosphorylation in *Pkn1*$^{-/-}$ cerebella protein lysates (Supplemental Figure 5A) and in immunofluorescence stainings (Figure 5, B and C). AKT phosphorylation levels were particularly increased in areas and developmental stages of axonal outgrowth and maturation of Cgc and dendritic outgrowth and maturation of PC. At P8 *Pkn1*$^{-/-}$ animals showed higher AKT phosphorylation in the PF-forming Cgc of the pre-migratory EGL, where Cgc start extending axons, as well as in the IGL (Figure 5B). At P15, higher AKT phosphorylation was found in the IGL and in PC dendrites (Figure 5C). In agreement with greater AKT activity we found increased NeuroD2 protein levels in *Pkn1*$^{-/-}$ cerebellar protein extracts (Figure 5D). There were no differences in AKT phosphorylation or NeuroD2 levels in adult animals (Supplemental

Figure 5, B and C), showing a development-specific effect of *Pkn1* knockout on AKT and NeuroD2.

These exciting results show for the first time that PKN1 controls AKT phosphorylation and NeuroD2 expression during cerebellar development in vivo, thereby explaining the defective PF-PC synapse formation and reduced Cbln1 expression levels upon *Pkn1* knockout.

Interestingly we also found that the enlarged dendritic caliber of *Pkn1*$^{-/-}$ PC could be reduced to WT levels upon incubation of organotypic slices with the AKT antagonist MK-2206, showing that PKN1 also controls PC dendritic caliber upstream of AKT (Supplemental Figure 5D). Therefore, we cannot exclude a PC-dependent defect, due to dendritic thickening upon *Pkn1* knockout that further weakens PF-PC synapse formation.

Adult Pkn1$^{-/-}$ *animals show cerebellar degeneration.* Several other studies have related a defective PF-PC synapse formation to a degeneration of Cgc and a late-onset loss of PC (22, 37). As compared to WT mice adult (3-9 month old) *Pkn1*$^{-/-}$ mice still displayed a similar cerebellar foliation pattern, but *Pkn1*$^{-/-}$ animals had smaller cerebella, as seen in a smaller sagittal vermis areas (Figure 6, A and B), with a thinner IGL (Figure 6, A and C) and ML (Figure 6, A and D). The facts that the proliferative layer of the EGL in young animals was similar between both genotypes (Supplemental Figure 6A) and that there were no ectopic NeuN-positive cells in the ML of adult *Pkn1*$^{-/-}$ cerebella (Supplemental Figure 6B) rule out a defective proliferation/migration of *Pkn1*$^{-/-}$ Cgc as the underlying mechanism. In further agreement with a defective PF-PC synapse formation, we saw no significant PC degeneration in 3-9 month old animals, but we found a late-onset loss of PC in *Pkn1*$^{-/-}$ mice older than 15 month (Figure 6E).

Adult *Pkn1*$^{-/-}$ still showed abnormal CF innervation, as seen in a significantly higher ratio of VGlut2/VGlut1 protein levels (Figure 6F) and increased VGlut2-staining (Figure 6G). In WT animals, VGlut2-stained CF terminals showed a reduction in the number of varicosities from the proximal part of the PC dendrite to the distal part (Figure 6G and Supplemental Figure 6C). This was not seen in *Pkn1*$^{-/-}$ animals, where the number of varicosities remained the same throughout the entire innervation depth of CF (Figure 6G and Supplemental Figure 6C). Additionally, PC of adult *Pkn1*$^{-/-}$ animals still had thicker dendrites (Supplemental Figure 6D), showing that *Pkn1* knockout-mediated defects of CF elimination and dendritic outgrowth persist throughout life.

Behavioral phenotyping of adult Pkn1$^{-/-}$ *mice reveals an ataxia-like phenotype.* Considering the important role of the cerebellum in balance and motor control we tested a cohort of adult (4-9 month) WT and *Pkn1*$^{-/-}$ mice in a set of refined motor behavior tests. *Pkn1*$^{-/-}$ mice showed an abnormal performance in the vertical pole test. While the majority of WT mice turned around and climbed down, most *Pkn1*$^{-/-}$ mice fell down, slid sideways or froze on the pole (Figure 7A), indicating balance and motor coordination problems. In line with this, *Pkn1*$^{-/-}$ mice were slower than WT mice in crossing a horizontal beam (Figure 7B) and showed more slips and balance coordination problems than WT mice in the ledge test (Figure 7C). Moreover *Pkn1*$^{-/-}$ mice exhibited hindlimb clasping, a sign of neurodegeneration (38), with most animals having one hindlimb partly retracted towards the body (Figure 7D). While the grip strength in the wire hang test was not different between the groups, the hindlimb grip duration was significantly reduced in *Pkn1*$^{-/-}$ mice, with most mice turning in circles and not being able to grab the wire properly (Figure 7E). Footprint analysis further indicated that *Pkn1*$^{-/-}$ mice preferred tip toe walking and showed a reduced toe spread score (Figure 6F). General locomotion in the open field test was similar between WT and *Pkn1*$^{-/-}$ mice (Supplemental Figure 7A). Likewise, anxiety-related behavior tested in the elevated plus maze, was not affected by *Pkn1* knockout

(Supplemental Figure 7B). Therefore, these behavioral tests revealed that *Pkn1*$^{-/-}$ mice show normal locomotor activity but have problems with balance and motor coordination and display signs of mild ataxia, such as hindlimb clasping and gait abnormalities. Interestingly the behavioral abnormalities of *Pkn1*$^{-/-}$ mice start before an obvious PC loss (Figure 6E) suggesting synaptic dysfunctions and Cgc degeneration, rather than PC degeneration as the underlying mechanism**.**

Discussion

Data presented here shed light on the largely unknown brain-specific functions of PKN1. We demonstrate that PKN1 is an important gatekeeper of intrinsic AKT activity during cerebellar development in vivo. We propose a mechanism by which PKN1-mediated AKT inhibition during PF-growth (P4-P15) results in a reduction of NeuroD2 levels and a subsequent increase in presynaptic specifications and Cbln1 expression in Cgc, which is essential for a correct PF-PC synapse formation and cerebellar long-term function.

Accordingly, *Pkn1*$^{-/-}$ animals have an impaired developmental regression of CFs, persistent multiple CF innervation and a reduced spontaneous ePSC frequency of PC, all indicative of a defective PF-PC synapse formation (Figure 1). Spontaneous PC activity in vitro is highly temperature sensitive and is inhibited at room temperature (25), therefore ePSCs recorded in our setting most likely arise from extrinsic input. Since the ratio of PF to CF synapses in the PC is in the order of 150:1 (39), it is generally assumed that most spontaneous ePSCs reflect PF activity (26, 27). Defective CF elimination and reduced spontaneous PC activity are also seen in animals lacking the genes encoding for *Cbln1* or *GluD2*, both of which are needed for a correct PF-PC synapse formation (22, 28, 37). Interestingly we found a reduced Cbln1 expression in *Pkn1*$^{-/-}$ animals, while GluD2 levels were only marginally affected, pointing towards a presynaptic Cgc-specific defect in PF-PC synapse formation.

Using in vitro Cgc cultures we could show that *Pkn1* knockout leads to enhanced AKT phosphorylation and subsequently higher NeuroD2 protein levels. Cbln1 and NeuroD2 levels are reciprocally regulated by AKT in vitro, with decreased NeuroD2- and increased Cbln1 levels upon AKT inhibition, further showing that in Cgc AKT is involved in controlling presynaptic differentiation. Subsequently, *Pkn1* knockout results in enhanced axonal outgrowth and reduced presynaptic differentiation in Cgc in vitro, both of which could be restored to WT levels upon inhibition of AKT. In line with our in vitro data *Pkn1*$^{-/-}$ animals showed pronounced AKT phosphorylation and higher NeuroD2 levels at developmental stages critical for PF growth and synapse maturation. Throughout cerebellar development NeuroD2 is only expressed in Cgc and ML interneurons, but not in PC (40, 41), and due to the relatively low ML interneuron numbers compared to Cgc, our analysis of protein extracts mainly reflects Cgc protein levels. NeuroD2 levels are particularly high during phases of axon growth where it prevents premature presynaptic maturation, but are degraded with increasing developmental maturation in order to drive presynaptic differentiation (30). Accordingly, NeuroD2 expression is tightly controlled since an increase in NeuroD2 decreases cell-intrinsic neuronal excitability (42). Our data offer pioneer evidence on a developmentally regulated PKN1-AKT axis that controls NeuroD2 levels and subsequently the precise balance between axonal growth and presynaptic differentiation of Cgc. Deletion of *Pkn1* therefore interferes with the correct PF-PC synapse formation (Figures 1-5) and results in cerebellar atrophy in adult animals (Figures 6 and 7).

The truncated C-terminal fragment of PKN1 enhances NeuroD2-mediated transcription in vitro and in mammalian cells overexpressing both proteins (43), therefore we cannot exclude that despite higher NeuroD2 protein levels in *Pkn1*$^{-/-}$ cerebella, the lack of PKN1 additionally affects NeuroD2 function. However, the fact that *Pkn1*$^{-/-}$ Cgc show a reduced density of presynaptic sites, a typical effect of NeuroD2 (30), points towards normal NeuroD2 activity.

Many neurological disorders have been linked with aberrant AKT signaling caused by germline mutations of certain tumor suppressor genes such as phosphatase and tensin homolog (*Pten*) or tuberous sclerosis proteins 1 and 2 (*Tsc2/Tsc1*) (44-46). Interestingly a partial-knockout of disabled homolog 2-interacting protein (*Dab2ip*), a molecule that shifts the balance of phosphatidylinositol 3-kinase (PI3K)/AKT-mediated cell survival towards apoptosis signal-regulating kinase 1 (ASK1)-mediated apoptosis, has a similar phenotype to *Pkn1*$^{-/-}$ mice (47). *Dab2ip* knockdown mice show aberrant PC dendrite maturation and a defective balance of CF/PF synaptic markers. *Pkn1*$^{-/-}$ mice also show some overlapping features with mice with a deletion of *Pten* (48-50). These include increased AKT phosphorylation, abnormal axonal outgrowth, enhanced presynaptic spacing, dendritic thickening, reduction of ML thickness, degeneration of PC and deficits in motor coordination (48-50). However, *Pkn1*$^{-/-}$ and *Pten*$^{-/-}$ phenotypes differ in other aspects such as brain enlargement and enlarged cell somata. The tight developmental regulation of PKN1-mediated AKT suppression (P4-P15, Supplemental Figure 5A and Figure 5) may serve as direct explanation for this discrepancy. Despite the rapidly increasing literature on AKT signaling and neurodevelopment, this is, to our knowledge, the first report linking developmental AKT activity with NeuroD2 levels and PF-PC synapse formation, and we offer PKN1 as a regulator of this pathway. The detailed elucidation of the molecular mechanism of AKT-mediated increase in NeuroD2 protein levels, such as if AKT enhances NeuroD2 expression via enhancement of neurogenin1 or NeuroD1 transcriptional activity (35, 36, 51), or else protects its proteolytic degradation, remains to be solved in future investigations.

Another well-characterized effect of a defective PF-PC synapse formation is a late-onset degeneration of Cgc and PC (22, 37). In agreement with that we show that the long-term effect of *Pkn1* knockout results in cerebellar shrinkage, PC degeneration and is accompanied by gait abnormalities, hind limp clasping and motor coordination problems (Figures 6 and 7), reminiscent of mild cerebellar ataxia (18). Interestingly, recent studies have connected microdeletions on chromosome 19p13.12 including *PKN1* to human cerebellar hypoplasias and psychomotor delays (52-55). It has therefore been suggested that one or more of the genes on chromosome 19p13.12 have a role in the control of movements (55) and our results establish *PKN1* as a promising new candidate gene for this.

Methods

Animals. The generation of *Pkn1* knockout mice (*Pkn1*$^{-/-}$ mice) has been described recently (17). Mice were backcrossed to C57BL/6N for more than 8 generations. C57BL/6N wildtype (WT) and C57BL/6N *Pkn1*$^{-/-}$ animals were derived from the same heterozygous crosses and then bred separately, but kept under same housing and experimental conditions in the same room. C57BL/6N were derived from Jackson Laboratory.

Behavioral phenotyping. Experiments were performed in a cohort of adult (3-9 month) WT (n = 11) and *Pkn1*$^{-/-}$ (n = 12) animals between 8 am and 1 pm.

Hindlimb clasping. Mice were lifted for 10-20 s by grasping their tail and movement of hindlimbs was scored as previously described (56). Hindlimb clasping was assessed 3 times; the mean score was calculated and rounded up or down to the full score. In case of 0.5 or 1.5 the score was downgraded to 0 or 1.

Ledge test. For the ledge test mice were lifted from their homecage and placed on another cage ledge, as described previously (56). The test was repeated twice, the mean score of both performances was calculated and rounded up or down to the full score. In case of 0.5 or 1.5 the score was downgraded to 0 or 1.

Pole climb. The task for the mice in this test was to turn around and climb down from the top of a vertical pole (1 cm diameter, 60 cm height) within 120 s. The behavior on the pole (climbing down, sliding down sideways, freezing on the column for more than 120 s or falling down) was assessed in three different trials and the percentage of each behavior for each mouse was analyzed.

Beam walk. Motor coordination and balance were assessed by measuring the ability of the mice to traverse a narrow 18 mm wide, 9 mm high, 2 m long beam. Mice were placed in the middle, 70 cm above the ground. Illumination was set to 150 lux. The latency to traverse the beam to the safety platform was recorded for two trials and the mean was calculated.

Wire hang. The animal was placed on a wire cage lid, which was then inverted and suspended above the home cage after a modified method (57). The cage lid was kept at 40 cm above a cage filled with soft material. The latency for each animal to release the grip with a cut-off time of 150 s as well as the hindlimb grip duration was recorded. The latter one was performed on video recordings of 9 WT and 12 *Pkn1*$^{-/-}$ animals.

Footprint analysis. The entire forelimbs of mice (paw and toes) were painted in red body paint and the entire hindlimbs were painted in blue body paint. Mice were released onto a white paper cardboard into a metal tunnel (6x70 cm) and allowed to walk to the other end into a safe cage. Tip toe walking was assessed by making sure that the mice can walk on the whole foot (paw and toes) and then scoring the gait for how they prefer to walk (tip toes or whole foot). The toe spread score was calculated by assigning values between 0 (narrowest spread) to 2 (widest spread).

Paraformaldehyde (PFA) perfusion. Mice were deeply anesthetized by an overdose of thiopental (150 mg/kg) and brains were fixed by transcardial perfusion with PBS (50 mM phosphate buffered saline, pH 7.2; 2 min) followed by 4% PFA in PBS (10 min).

Preparation of cerebellar granule cells. Cgc were prepared as described previously (58). Cells were kept in Neurobasal medium (Thermo Fisher Scientific) supplemented with 1% Penicillin/Streptomycin/Glutamine (Sigma-Aldrich), 2% B-27 (Thermo Fisher Scientific) and an additional 20 mM KCl. Coverslips and dishes were coated with Poly-L-Ornithine or Poly-L-Lysin (2 h-overnight, Sigma-Aldrich) and for coverslips Laminin (10 µg/ml, Sigma-Aldrich) was subsequently added for 2-3 h at 37°C. MK-2206 (Santa Cruz) was added 2-3 h after preparation.

Transfections of cerebellar granule cells. Nucleofection (Lonza) of Cgc was performed as described previously (59) with 5 µg plasmid DNA, and if indicated together with 3 µg pmax *GFP* plasmid (Lonza) using program G-013. Human (h)*PKN1* was purchased from GeneCopoeia, (Rockville, USA) and subcloned into the mammalian expression vector pEF-neo. For Lipofectamine transfections 2 µl Lipofectamine (Thermo Fisher Scientific) and 0.9 µg plasmid DNA were mixed with Neurobasal medium and added to coverslips for 6-8 h. The medium was then exchanged for the preconditioned culture medium and cells were analyzed after 48 h. *Akt123*- and control siRNAs were purchased from Dharmacon. For siRNA transfections 101 nM of each *Akt* siRNA (303 nM in total) and 303 nM control, non targeting siRNAs were transfected with programs G-013 or O-005, both of which yielded similar results. Using higher siRNA concentrations resulted in cell death upon *Akt* knockdown (data not shown). Transfections of the same Cgc preparation with two different programs were counted as separate experiments.

Cryosectioning. P1, P4, P8, P15 and adult brains were fixed in 4% PFA for 2.5 (P1, P4 and P8), 5 h (P15), overnight (adult brains) or by PFA-perfusion. Brains were incubated in a sucrose gradient (10% sucrose for 2 h, 20% sucrose overnight and 30% sucrose for a minimum of two days), embedded in optimal cutting temperature compound (Thermo Fisher Scientific) and stored at -80°C until analysis. 20 µm thick sections were cut with a cryostat (CM1950, Leica), transferred onto lysine-coated coverslips (Sigma-Aldrich) and allowed to dry for 2 h at room temperature for further analysis or stored at -20°C. In order to ensure comparable results age-matched WT and *Pkn1*$^{-/-}$ sections were prepared on the same day and transferred onto the same coverslip.

Immunofluorescence staining. Cells were fixed (4% PFA 15 min, Methanol 30 s at -20°C), permeabilized (0.3% Triton-X-100, 15 min) and blocked (1% BSA, 2% goat serum, 1 h). For cerebellar sections permeabilization was 30 min and a higher blocking solution was used (10% goat serum, 2% BSA, 1 h). For VGlut2- and pAKT T308-staining of cerebellar sections we performed antigen retrieval in a 10 mM sodium citrate buffer pH6 with 0.05% Tween 20 (100°C for 10 min). Primary antibodies (diluted in 0.1% Triton-X-100, 1% BSA, 2% goat serum in PBS) were added at 4°C overnight. After washing in PBS, secondary antibodies (goat-anti rabbit Alexa-488, and goat anti-mouse Alexa-555) were added for 2-4 h at room temperature. Coverslips/sections were washed in PBS and embedded in Mowiol (Sigma-Aldrich). Images were taken with a widefield (Axio, Zeiss) or laser scanning confocal microscope (SP5, Leica). For widefield microscopy the same exposure time and for confocal microscopy the same laser intensity was used to compare WT and *Pkn1*$^{-/-}$ sections. Confocal stacks were merged in ImageJ (Rasband, W.S., U. S. National Institutes of Health) and for better visualization the intensity of Calbindin and VGlut-2 stainings was increased to the same extent using ImageJ. For comparison of pAKT intensity brain sections of WT and *Pkn1*$^{-/-}$ animals were prepared on the same day, transferred onto the same coverslip and stained with the same antibody solution. Confocal images of at least three independent experiments, taken at the same exposure time are shown.

Analysis of cerebellar morphology. All analyses were performed in the cerebellar vermis area of cerebellar lobule IV/V in a blinded manner using ImageJ. The mean vermis area was calculated from 2-6 sections/animal. The IGL thickness (3-5 measurements of 2-5 sections/animal) and ML (3-5 measurements of 2-5 sections/animal) thickness was measured at the thickest part of the cerebellar lobule IV/V. The VGlut2/ML ratio was determined by 4-14 measurements of 1-2 sagittal sections/animal. Perisomatic VGlut2-staining was scored by two experimenters in 1-2 confocal images/animal.

Measurement of axonal length and presynaptic spacing. Cgc, grown on Laminin-coated coverslips were fixed at indicated timepoints and stained for TAU. Pictures were manually cleaned from background noise using ImageJ. Incomplete neurons as well as neurons with axons that crossed other axons (in that case the neuron with the shorter axon, or the one which crossed more than two other axons was deleted) were erased. A minimum of 70 cells/coverslip (DIV1) and 20 cells/coverslip (DIV7) and a minimum of 21 GFP-positive transfected cells were analyzed with WIS Neuromath (60, 61). The number of presynaptic varicosities per 50 µm axonal section was determined by 1-4 measurements per axon from 24-42 cells/preparation.

Measurement of pAKT and NeuroD2 intensity in transfected cerebellar granule cells. $Pkn1^{-/-}$ Cgc grown on Laminin were Lipofectamine-transfected with h*PKN1* on DIV5 and fixed and stained for HA and pAKT T308 on DIV7. For NeuroD2 intensity measurements Nucleofection was used to introduce h*PKN1* in *$Pkn1^{-/-}$* Cgc immediately after preparation and cells were then kept for DIV4 on Laminin-coated coverslips. Cells were fixed and stained for NeuroD2 and HA. Images were taken with a widefield (Axio, Zeiss) microscope and mean pAKT or NeuroD2 levels were measured with ImageJ in the transfected (HA-positive) cell and the surrounding untransfected cells. Between 8-32 transfected cells were analyzed and averaged per experiment. The average pAKT or NeuroD2 intensity in untransfected cells was calculated from 3-15 cells surrounding the transfected cells per picture.

Electrophysiology. The age for spontaneous ePSC recordings was P13-P15 (WT average age of 13.7, *$Pkn1^{-/-}$* mice average age of 15) and for CF-induced ePSCs P15-P17 (WT average age of 15.7, *$Pkn1^{-/-}$* mice average age of 15.2). Animals were anesthetized (isofluorane) and decapitated. Brains were gently removed and immediately chilled (~ 0°C) in high-glucose artificial cerebrospinal fluid (HiGluc-aCSF) containing (in mM): NaCl, 125; $NaHCO_3$, 26; D-glucose, 25; KCl, 2.5; NaH_2PO_4, 1.43; $CaCl_2$, 2; $MgCl_2$, 1. The aCSF pH was adjusted to 7.4 with a saturating carbogen mix (95 O_2/5% CO_2). 300 μm thick parasagittal cerebellar slices were cut along the vermis with a vibratome (Leica VT1200S) in ice-cold HiGluc-aCSF. Slices were thereafter allowed to recover for at least 30 minutes in HiGluc-aCSF, bubbled with 95% O_2/5% CO_2, at room temperature until required and for a maximum of 8 h. Whole-cell patch recordings were performed on visually identified PC in Lobulus IV/V by using a 20X water immersion objective (Olympus) with an additional 2X magnifier as described previously (62). Briefly, slices were transferred to a submersion-style recording chamber mounted on a Olympus BXS1WI and superfused with standard aCSF, continuously bubbled with 95% O_2/5% CO_2 at room temperature, comprising (in mM): NaCl, 125; $NaHCO_3$, 26; D-glucose, 10; KCl, 2.5; NaH_2PO_4, 1.43; $CaCl_2$, 2; $MgCl_2$, 1. The aCSF had an osmolality of 310 mOs/kg. Patch pipettes were pulled from borosilicate capillaries (GB120F-10, Science Products, Germany) with a Sutter P-1000 puller, the resistance was typically 2–5 mOhm when filled with internal solution consisting of (in mM): K-gluconate, 132; EGTA/KOH, 1; $MgCl_2$, 2; NaCl, 2; Hepes/KOH, 10; Mg-ATP, 2; GTP, 0.5. The pH was adjusted to 7.2 – 7.25 with KOH and the osmolality was 280 - 285 mOs/kg. Recordings were obtained using a Multiclamp 700B amplifier and displayed with pClamp (Molecular Devices). In whole-cell configuration (holding potential -70 mV), series resistances (Rs) were typically around 10-15 MΩ. Cells were allowed to equilibrate for 10 minutes before recording. Evoked CF inputs were triggered with a stimulation electrode filled with aCSF (resistance ~0.5 mOhm) that was placed 50-70 μm away from the recorded PC soma in the granule cell layer. The unipolar square pulses with durations of 0.2 ms were delivered at 0.1 Hz via a constant current stimulus isolator (World Precision Instruments A365). Stimulation current amplitudes were between 5 μA and 100 μA. At least three discrete steps above triggering threshold with a step-size of 10 μA were recorded in each cell. The CF synaptic inputs to the PC were recorded at room temperature at a holding potential of -70 mV, low-pass filtered at 10 kHz and sampled at 20 kHz. Data analysis was done in Matlab

(Mathworks) and traces were analyzed by two different, blinded experimenters. Spontaneous excitatory postsynaptic currents (ePSC) and inhibitory postsynaptic currents (iPSC) were recorded at room temperature, low-pass filtered at 10 kHz and sampled at 20 kHz, traces were low-pass filtered after recordings at 1–4 kHz and analyzed with Clampfit module in pClamp.

Western blotting. Protein extracts and western blotting was performed as described previously (59). Primary antibodies were added over night in 5% BSA in TBS-T at 4°C and secondary antibodies (LiCor, anti-mouse 680 nm, shown in red and anti-rabbit 800 nm, shown in green) or HRP-tagged antibodies were added for 90 min in 5% Milk in TBS-T. After washing in TBS-T membranes were imaged and analyzed with Odyssey infrared Imager (LiCor) or ECL detection as described previously (63).

Antibodies. Clone numbers, where known, and catalog numbers (#) are provided in brackets. The pAKT T308 antibody (#SAB4300043, further validated with MK-2206 in Cgc, not shown) was from Sigma-Aldrich. The following antibodies were from Cell signaling: ERK1/2 (#9102), GAPDH (D16H11, #5174), HA-Tag (C29F4, #3724), NeuN (D4G40, #24307), pAKT S473 (western blotting, D9E, #4060), pERK1/2 (#9101), pan-AKT (western blotting, 40D4, #2920), Synapsin-I (D12G5, #5297), TAU (Tau46, #4019). α-Tubulin (DM1A, #ab80779), Calbindin (#ab11426), Calbindin (CB-955, #ab82812), Cerebellin 1 (EPR13649, #ab181379), Ki-67 (#ab15580), pAKT S473 (immunofluorescence staining, EP2109Y, #ab81283, further validated with MK-2206 in Cgc, not shown), AKT1/2/3 (immunofluorescence staining and western blotting, EPR16798, #ab179463) and VGlut2 (8G9.2, #ab79157) were from Abcam. HA.11 (Clone 16B12, #MMS-101P) was from Covance. VGlut1 (#48-2400), goat-anti rabbit Alexa-488 (#A11070) and goat anti-mouse Alexa-555 (#A21425) was purchased from Thermo Fisher Scientific and GluD2 (D-9, #sc-393437) and NeuroD2 (G-10, #sc-365896) were from Santa Cruz. PKN1 (clone 49/PRK1, #610687) was from BD Transduction Laboratories. The secondary antibodies for the Odyssey infrared Imager, IR680 LT mouse (#92668020) and IR800CW (#92632211) were purchased from Licor.

Statistics. No statistical methods were used to predetermine sample sizes, but our sample sizes are similar to those reported in previous publications and typically had a statistical power sufficient to detect differences on the order of our effect sizes. Normal distributions of data were presumed but not formally tested, equal variances were tested and if not met an unpaired two-tailed t-test with Welch's correction was used. All data are presented as individual *n*-values with or as mean±SEM. For behavioral and histochemical analysis *n*-values refer to different animals from at least three different litters. For all cell culture experiments *n*-values refer to animals from different litters or transfections. For comparison of two independent groups a two-tailed unpaired t-test was used and for comparison of two dependent groups a two-tailed paired t-test was employed. For comparison of three or more groups one-way ANOVA with Newman-Keuls multiple comparison test was used and for comparison of two variables of two groups a two-way ANOVA was used. For comparison of the different behavior on the pole climb, scores and multiple/singe CF innervation a chi-square test was used. *P*-values smaller than 0.05 were considered as statistically significant. All analyses were performed in Graphpad prism 5 and 7.

Study approval. For all studies employing adult animals, male mice were used and all procedures were approved by the Austrian Animal Experimentation Ethics Board in compliance with the European Convention for the Protection of Vertebrate Animals Used for Experimental and Other Scientific Purposes ETS no.: 123/. (BMWFW-66.011/0040-WF/V/3b/2016). Every effort was taken to minimize the number of animals used. The study was designed in compliance with the ARRIVE guidelines. Blinding was always performed by a third party and every Figure legend clearly states if analysis was performed in a blinded or non-blinded manner.

Author contributions

GB-B and SzN developed the study concept and design. SzN performed immunoblotting, immunohistochemistry, cell and slice culture experiments. RE and SzN performed studies on cerebellar morphology. F.F. and G.B. performed recombinant DNA work. AC and PP attributed the *Pkn1*$^{-/-}$ knockout mice. CS designed and SzN, SC, CS, RE and GB-B performed the animal behavior experiments. LZ, HS and AK performed the electrophysiological experiments. SzN and GB-B supervised the project and wrote the manuscript with critical input from all authors. GB-B was the responsible coordinator of the project. All authors approved the manuscript.

Acknowledgements

We thank K. Thuille, T. Gruber, M. Klose, N. Posch, C. Stichlberger, M. Offterdinger, M. Kind for technical support and B. Benedetti and C. Bandtlow for helpful discussions. We thank M.J. Woolley for stylistic and editorial assistance. This study was funded by the Austrian Science Fund ((P 26002 B-24 (GB-B), P30324-B21 (GB), P30430 (CS), P29359 (AK)) and the Christian Doppler Society (GB).

References

1. Mukai H, Muramatsu A, Mashud R, Kubouchi K, Tsujimoto S, Hongu T, et al. PKN3 is the major regulator of angiogenesis and tumor metastasis in mice. *Sci Rep.* 2016;6:18979.
2. Ostrovskyi D, Rumpf T, Eib J, Lumbroso A, Slynko I, Klaeger S, et al. Tofacitinib and analogs as inhibitors of the histone kinase PRK1 (PKN1). *Future Med Chem.* 2016;8(13):1537-51.
3. Mukai H, and Ono Y. A novel protein kinase with leucine zipper-like sequences: its catalytic domain is highly homologous to that of protein kinase C. *Biochemical and biophysical research communications.* 1994;199(2):897-904.
4. Hashimoto T, Mukai H, Kawamata T, Taniguchi T, Ono Y, and Tanaka C. Localization of PKN mRNA in the rat brain. *Brain research Molecular brain research.* 1998;59(2):143-53.
5. Kawamata T, Taniguchi T, Mukai H, Kitagawa M, Hashimoto T, Maeda K, et al. A protein kinase, PKN, accumulates in Alzheimer neurofibrillary tangles and associated endoplasmic reticulum-derived vesicles and phosphorylates tau protein. *J Neurosci.* 1998;18(18):7402-10.
6. Palmer RH, Ridden J, and Parker PJ. Cloning and expression patterns of two members of a novel protein-kinase-C-related kinase family. *European journal of biochemistry / FEBS.* 1995;227(1-2):344-51.
7. Flynn P, Mellor H, Palmer R, Panayotou G, and Parker PJ. Multiple interactions of PRK1 with RhoA. Functional assignment of the Hr1 repeat motif. *The Journal of biological chemistry.* 1998;273(5):2698-705.
8. Mukai H. The structure and function of PKN, a protein kinase having a catalytic domain homologous to that of PKC. *J Biochem (Tokyo).* 2003;133(1):17-27.

9. Mukai H, Miyahara M, Sunakawa H, Shibata H, Toshimori M, Kitagawa M, et al. Translocation of PKN from the cytosol to the nucleus induced by stresses. *Proc Natl Acad Sci U S A.* 1996;93(19):10195-9.

10. Takahashi M, Mukai H, Toshimori M, Miyamoto M, and Ono Y. Proteolytic activation of PKN by caspase-3 or related protease during apoptosis. *Proc Natl Acad Sci U S A.* 1998;95(20):11566-71.

11. Manser C, Stevenson A, Banner S, Davies J, Tudor EL, Ono Y, et al. Deregulation of PKN1 activity disrupts neurofilament organisation and axonal transport. *FEBS letters.* 2008;582(15):2303-8.

12. Sumioka K, Shirai Y, Sakai N, Hashimoto T, Tanaka C, Yamamoto M, et al. Induction of a 55-kDa PKN cleavage product by ischemia/reperfusion model in the rat retina. *Invest Ophthalmol Vis Sci.* 2000;41(1):29-35.

13. Ueyama T, Ren Y, Sakai N, Takahashi M, Ono Y, Kondoh T, et al. Generation of a constitutively active fragment of PKN in microglia/macrophages after middle cerebral artery occlusion in rats. *Journal of neurochemistry.* 2001;79(4):903-13.

14. Okii N, Amano T, Seki T, Matsubayashi H, Mukai H, Ono Y, et al. Fragmentation of protein kinase N (PKN) in the hydrocephalic rat brain. *Acta Histochem Cytochem.* 2007;40(4):113-21.

15. Thauerer B, zur Nedden S, and Baier-Bitterlich G. Vital role of protein kinase C-related kinase in the formation and stability of neurites during hypoxia. *J Neurochem.* 2010;113(2):432-46.

16. Thauerer B, Zur Nedden S, and Baier-Bitterlich G. Protein Kinase C-Related Kinase (PKN/PRK). Potential Key-Role for PKN1 in Protection of Hypoxic Neurons. *Curr Neuropharmacol.* 2014;12(3):213-8.

17. Quetier I, Marshall JJ, Spencer-Dene B, Lachmann S, Casamassima A, Franco C, et al. Knockout of the PKN Family of Rho Effector Kinases Reveals a Non-redundant Role for PKN2 in Developmental Mesoderm Expansion. *Cell Rep.* 2016.

18. Cendelin J. From mice to men: lessons from mutant ataxic mice. *Cerebellum Ataxias.* 2014;1:4.

19. Hoxha E, Tempia F, Lippiello P, and Miniaci MC. Modulation, Plasticity and Pathophysiology of the Parallel Fiber-Purkinje Cell Synapse. *Front Synaptic Neurosci.* 2016;8:35.

20. Ichikawa R, Sakimura K, and Watanabe M. GluD2 Endows Parallel Fiber-Purkinje Cell Synapses with a High Regenerative Capacity. *J Neurosci.* 2016;36(17):4846-58.

21. Watanabe M, and Kano M. Climbing fiber synapse elimination in cerebellar Purkinje cells. *Eur J Neurosci.* 2011;34(10):1697-710.

22. Hirai H, Pang Z, Bao D, Miyazaki T, Li L, Miura E, et al. Cbln1 is essential for synaptic integrity and plasticity in the cerebellum. *Nat Neurosci.* 2005;8(11):1534-41.

23. Lin H, Magrane J, Clark EM, Halawani SM, Warren N, Rattelle A, et al. Early VGLUT1-specific parallel fiber synaptic deficits and dysregulated cerebellar circuit in the KIKO mouse model of Friedreich ataxia. *Dis Model Mech.* 2017;10(12):1529-38.

24. Kano M, Hashimoto K, Kurihara H, Watanabe M, Inoue Y, Aiba A, et al. Persistent multiple climbing fiber innervation of cerebellar Purkinje cells in mice lacking mGluR1. *Neuron.* 1997;18(1):71-9.

25. Womack M, and Khodakhah K. Active contribution of dendrites to the tonic and trimodal patterns of activity in cerebellar Purkinje neurons. *J Neurosci.* 2002;22(24):10603-12.

26. Zhang B, Chen LY, Liu X, Maxeiner S, Lee SJ, Gokce O, et al. Neuroligins Sculpt Cerebellar Purkinje-Cell Circuits by Differential Control of Distinct Classes of Synapses. *Neuron.* 2015;87(4):781-96.

27. Ito-Ishida A, Miura E, Emi K, Matsuda K, Iijima T, Kondo T, et al. Cbln1 regulates rapid formation and maintenance of excitatory synapses in mature cerebellar Purkinje cells in vitro and in vivo. *J Neurosci.* 2008;28(23):5920-30.

28. Uemura T, Lee SJ, Yasumura M, Takeuchi T, Yoshida T, Ra M, et al. Trans-synaptic interaction of GluRdelta2 and Neurexin through Cbln1 mediates synapse formation in the cerebellum. *Cell.* 2010;141(6):1068-79.

29. Matsuda K, Miura E, Miyazaki T, Kakegawa W, Emi K, Narumi S, et al. Cbln1 is a ligand for an orphan glutamate receptor delta2, a bidirectional synapse organizer. *Science.* 2010;328(5976):363-8.

30. Yang Y, Kim AH, Yamada T, Wu B, Bilimoria PM, Ikeuchi Y, et al. A Cdc20-APC ubiquitin signaling pathway regulates presynaptic differentiation. *Science.* 2009;326(5952):575-8.

31. Shepherd GM, Raastad M, and Andersen P. General and variable features of varicosity spacing along unmyelinated axons in the hippocampus and cerebellum. *Proc Natl Acad Sci U S A.* 2002;99(9):6340-5.

32. Dajas-Bailador F, Bantounas I, Jones EV, and Whitmarsh AJ. Regulation of axon growth by the JIP1-AKT axis. *J Cell Sci.* 2014;127(Pt 1):230-9.

33. Wick MJ, Dong LQ, Riojas RA, Ramos FJ, and Liu F. Mechanism of phosphorylation of protein kinase B/Akt by a constitutively active 3-phosphoinositide-dependent protein kinase-1. *J Biol Chem.* 2000;275(51):40400-6.

34. Yasui T, Sakakibara-Yada K, Nishimura T, Morita K, Tada S, Mosialos G, et al. Protein kinase N1, a cell inhibitor of Akt kinase, has a central role in quality control of germinal center formation. *Proceedings of the National Academy of Sciences of the United States of America.* 2012;109(51):21022-7.

35. Wang L, Zhang ZG, Zhang RL, Jiao ZX, Wang Y, Pourabdollah-Nejad DS, et al. Neurogenin 1 mediates erythropoietin enhanced differentiation of adult neural progenitor cells. *J Cereb Blood Flow Metab.* 2006;26(4):556-64.

36. Darshit BS, and Ramanathan M. Activation of AKT1/GSK-3beta/beta-Catenin-TRIM11/Survivin Pathway by Novel GSK-3beta Inhibitor Promotes Neuron Cell Survival: Study in Differentiated SH-SY5Y Cells in OGD Model. *Mol Neurobiol.* 2016;53(10):6716-29.

37. Zanjani HS, Vogel MW, and Mariani J. Deletion of the GluRdelta2 Receptor in the Hotfoot Mouse Mutant Causes Granule Cell Loss, Delayed Purkinje Cell Death, and Reductions in Purkinje Cell Dendritic Tree Area. *Cerebellum.* 2016;15(6):755-66.

38. Chou AH, Yeh TH, Ouyang P, Chen YL, Chen SY, and Wang HL. Polyglutamine-expanded ataxin-3 causes cerebellar dysfunction of SCA3 transgenic mice by inducing transcriptional dysregulation. *Neurobiol Dis.* 2008;31(1):89-101.

39. Strata P, and Rossi F. Plasticity of the olivocerebellar pathway. *Trends Neurosci.* 1998;21(9):407-13.

40. Lin CH, Stoeck J, Ravanpay AC, Guillemot F, Tapscott SJ, and Olson JM. Regulation of neuroD2 expression in mouse brain. *Dev Biol.* 2004;265(1):234-45.

41. Miyata T, Maeda T, and Lee JE. NeuroD is required for differentiation of the granule cells in the cerebellum and hippocampus. *Genes Dev.* 1999;13(13):1647-52.

42. Chen F, Moran JT, Zhang Y, Ates KM, Yu D, Schrader LA, et al. The transcription factor NeuroD2 coordinates synaptic innervation and cell intrinsic properties to control excitability of cortical pyramidal neurons. *J Physiol.* 2016;594(13):3729-44.

43. Shibata H, Oda H, Mukai H, Oishi K, Misaki K, Ohkubo H, et al. Interaction of PKN with a neuron-specific basic helix-loop-helix transcription factor, NDRF/NeuroD2. *Brain Res Mol Brain Res.* 1999;74(1-2):126-34.

44. Lasarge CL, and Danzer SC. Mechanisms regulating neuronal excitability and seizure development following mTOR pathway hyperactivation. *Front Mol Neurosci.* 2014;7:18.

45. Orlova KA, and Crino PB. The tuberous sclerosis complex. *Ann N Y Acad Sci.* 2010;1184:87-105.

46. Franke TF. PI3K/Akt: getting it right matters. *Oncogene.* 2008;27(50):6473-88.

47. Qiao S, Kim SH, Heck D, Goldowitz D, LeDoux MS, and Homayouni R. Dab2IP GTPase activating protein regulates dendrite development and synapse number in cerebellum. *PLoS One.* 2013;8(1):e53635.

48. Cupolillo D, Hoxha E, Faralli A, De Luca A, Rossi F, Tempia F, et al. Autistic-Like Traits and Cerebellar Dysfunction in Purkinje Cell PTEN Knock-Out Mice. *Neuropsychopharmacology.* 2015.

49. Backman SA, Stambolic V, Suzuki A, Haight J, Elia A, Pretorius J, et al. Deletion of Pten in mouse brain causes seizures, ataxia and defects in soma size resembling Lhermitte-Duclos disease. *Nat Genet.* 2001;29(4):396-403.

50. Kwon CH, Zhu X, Zhang J, Knoop LL, Tharp R, Smeyne RJ, et al. Pten regulates neuronal soma size: a mouse model of Lhermitte-Duclos disease. *Nat Genet.* 2001;29(4):404-11.

51. Vojtek AB, Taylor J, DeRuiter SL, Yu JY, Figueroa C, Kwok RP, et al. Akt regulates basic helix-loop-helix transcription factor-coactivator complex formation and activity during neuronal differentiation. *Mol Cell Biol.* 2003;23(13):4417-27.

52. Bonaglia MC, Marelli S, Novara F, Commodaro S, Borgatti R, Minardo G, et al. Genotype-phenotype relationship in three cases with overlapping 19p13.12 microdeletions. *Eur J Hum Genet.* 2010;18(12):1302-9.

53. Gallant NM, Baldwin E, Salamon N, Dipple KM, and Quintero-Rivera F. Pontocerebellar hypoplasia in association with de novo 19p13.11p13.12 microdeletion. *Am J Med Genet A.* 2011;155A(11):2871-8.

54. Jensen DR, Martin DM, Gebarski S, Sahoo T, Brundage EK, Chinault AC, et al. A novel chromosome 19p13.12 deletion in a child with multiple congenital anomalies. *Am J Med Genet A.* 2009;149A(3):396-402.

55. Dale RC, Grattan-Smith P, Nicholson M, and Peters GB. Microdeletions detected using chromosome microarray in children with suspected genetic movement disorders: a single-centre study. *Dev Med Child Neurol.* 2012;54(7):618-23.

56. Guyenet SJ, Furrer SA, Damian VM, Baughan TD, La Spada AR, and Garden GA. A simple composite phenotype scoring system for evaluating mouse models of cerebellar ataxia. *J Vis Exp.* 2010(39).

57. Bonetto A, Andersson DC, and Waning DL. Assessment of muscle mass and strength in mice. *Bonekey Rep.* 2015;4:732.

58. zur Nedden S, Doney AS, and Frenguelli BG. Modulation of intracellular ATP determines adenosine release and functional outcome in response to metabolic stress in rat hippocampal slices and cerebellar granule cells. *J Neurochem.* 2014;128(1):111-24.

59. zur Nedden S, Tomaselli B, and Baier-Bitterlich G. HIF-1 alpha is an essential effector for purine nucleoside-mediated neuroprotection against hypoxia in PC12 cells and primary cerebellar granule neurons. *Journal of neurochemistry.* 2008;105(5):1901-14.

60. Galun M, Basri R, and Brandt A. Multiscale edge detection and fiber enhancement using differences of oriented means. *2007 Ieee 11th International Conference on Computer Vision, Vols 1-6.* 2007:722-9.

61. Rishal I, Golani O, Rajman M, Costa B, Ben-Yaakov K, Schoenmann Z, et al. WIS-NeuroMath enables versatile high throughput analyses of neuronal processes. *Dev Neurobiol.* 2013;73(3):247-56.

62. Benedetti B, Benedetti A, and Flucher BE. Loss of the calcium channel beta4 subunit impairs parallel fibre volley and Purkinje cell firing in cerebellum of adult ataxic mice. *Eur J Neurosci.* 2016;43(11):1486-98.

63. Thauerer B, Voegele P, Hermann-Kleiter N, Thuille N, de Araujo ME, Offterdinger M, et al. LAMTOR2-mediated modulation of NGF/MAPK activation kinetics during differentiation of PC12 cells. *PLoS One.* 2014;9(4):e95863.

Figures and legends

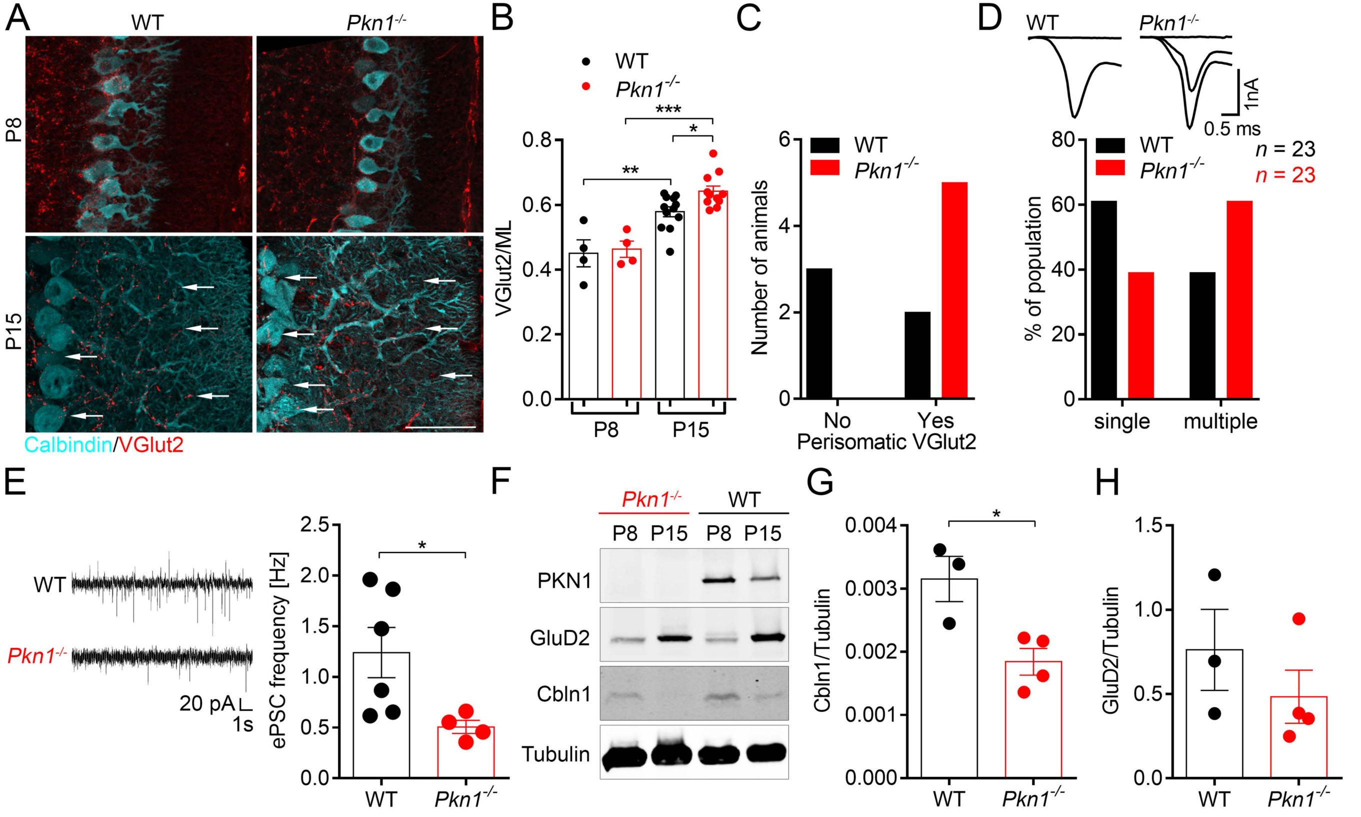

Figure 1. *Pkn1*$^{-/-}$ mice show a defective parallel fiber-Purkinje cell synapse formation during development. (**A**) Cerebellar vermis sections of P8-P15 old animals (n = 4-12, see Figure 1B-C for analysis). Arrowheads mark distal and perisomatic varicosities of VGlut2-stained CF. Scale bar represents 50 µm. (**B**) The ratio of the VGlut2-stained CF innervation depth [µm] to the ML thickness [µm] was analyzed (one-way ANOVA with Newman-Keuls multiple comparison test, $F(3,27) = 16.7$, $P < 0.0001$, post-test (*) $P < 0.05$, (**) $P < 0.01$, (***) $P < 0.001$; n = 4 WT/4 *Pkn1*$^{-/-}$ animals for P8, n = 12 WT/11 *Pkn1*$^{-/-}$ animals for P15 from 5-8 litters/group). (**C**) The score of PC perisomatic VGlut2-staining in P15 animals (chi-square test (1) = 4.286, (*) $P = 0.0384$, n = 5 WT/5 *Pkn1*$^{-/-}$ animals from 5 litters/group). (**D**) CF-induced ePSCs were recorded from PC in acute slices. With increasing stimulation strength ePSCs were obtained in an all-or-none fashion (single CF) or in two or more discrete steps (multiple CF) (chi-square test (1) = 9.68, (**) $P = 0.0019$, n = 23 WT/23 *Pkn1*$^{-/-}$ cells from 7 P15-P17 old animals/group). (**E**) Spontaneous PC ePSCs frequencies (two-tailed unpaired t-test with Welch's correction, $t(5) = 2.865$, (*) $P = 0.0352$, n = 6 WT/4 *Pkn1*$^{-/-}$ cells from 3-5 P13-P15 old animals/group). (**F**) Western blot analysis of Cbln1 and GluD2 levels (n = 3-4, see Figure 1G-H for analysis). (**G**) Analysis of the Cbln1/Tubulin ratio (two-tailed unpaired t-test, $t(5) = 3.365$, (*) $P = 0.0200$, n = 3 WT/4 *Pkn1*$^{-/-}$ extracts from 3-4 animals/group) and (**H**) GluD2/Tubulin ratio (two-tailed unpaired t-test, $t(5) = 1.016$, $P = 0.3561$, n = 3 WT/4 *Pkn1*$^{-/-}$ extracts from 3-4 animals/group) in P15 animals. Data is presented as individual n-values with mean±SEM. All analyses/experiments, except **F-H** were performed in a blinded manner.

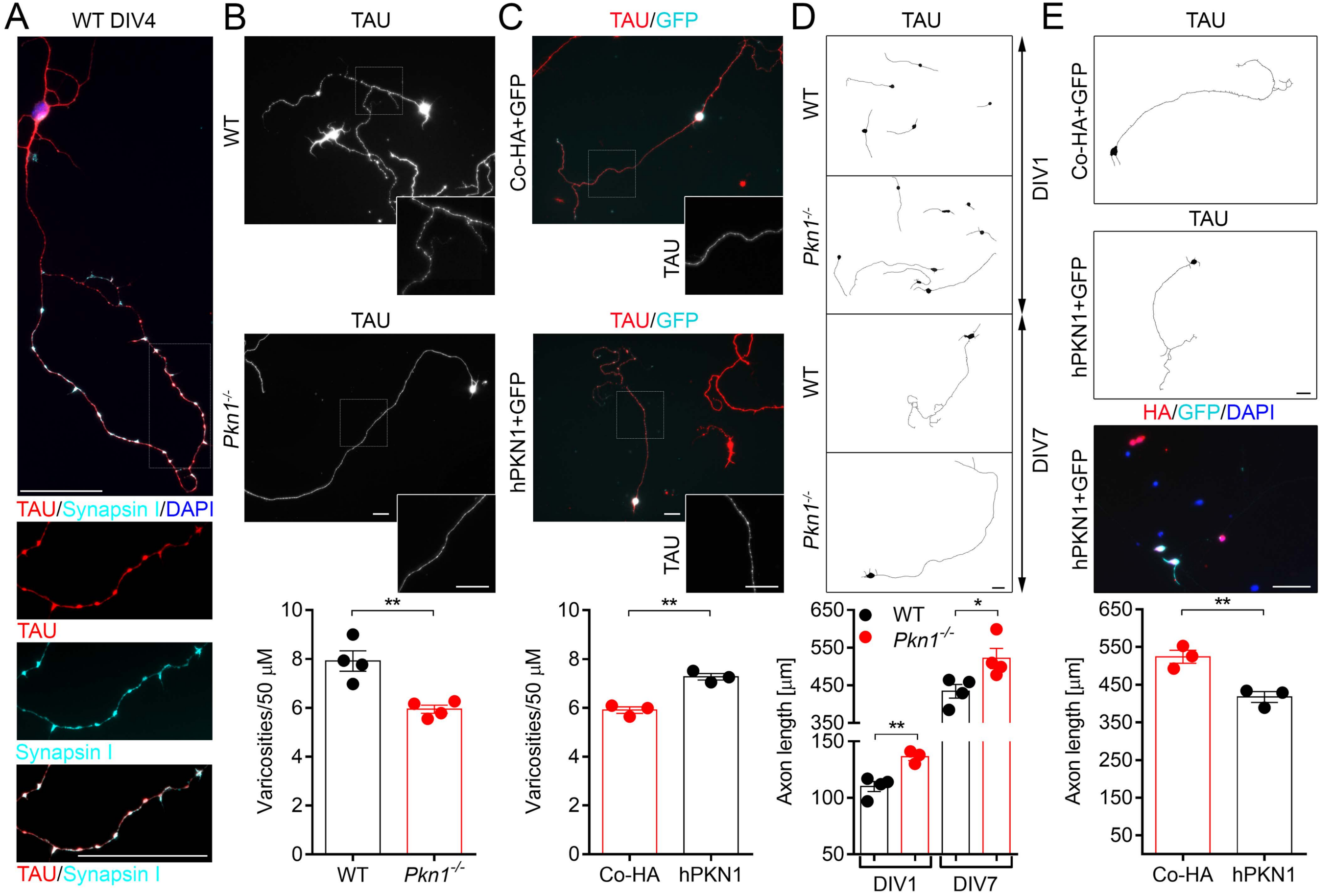

Figure 2. *Pkn1*$^{-/-}$ Cgc have a reduced density of presynaptic sites and enhanced axonal outgrowth. (**A**) In WT Cgc TAU-stained axonal en passant swellings colocalized with the presynaptic marker Synapsin I (images were taken at DIV4 and are representative of at least 3 separate experiments in WT and *Pkn1*$^{-/-}$ Cgc). (**B**) The number of en passant swellings (varicosities) per axonal section was analyzed in WT and *Pkn1*$^{-/-}$ Cgc at DIV7 (two-tailed unpaired t-test, $t(6) = 4.413$, (**) $P = 0.0045$, $n = 4$ WT/4 *Pkn1*$^{-/-}$ Cgc preparations from 4 litters/group). (**C**) *Pkn1*$^{-/-}$ Cgc were transfected with *GFP* together with a control HA-Plasmid (Co-HA) or human HA-tagged *PKN1* (h*PKN1*) and varicosities per axonal section were analyzed at DIV7 in GFP-expressing/TAU-stained Cgc (two-tailed unpaired t-test, $t(4) = 7.147$, (**) $P = 0.002$, $n = 3$ from 3 litters). (**D**) Axonal length after DIV1 (two-tailed unpaired t-test, $t(5) = 4.431$, (**) $P = 0.0068$, $n = 4$ WT/3 *Pkn1*$^{-/-}$ Cgc preparations from 3-4 litters/group) and DIV7 (two-tailed unpaired t-test, $t(6) = 2.692$, (*) $P = 0.0360$, $n = 4$ WT/4 *Pkn1*$^{-/-}$ Cgc preparations from 4 litters/group) in TAU-stained Cgc. (**E**) *Pkn1*$^{-/-}$ Cgc were transfected with *GFP* together with Co-HA or h*PKN1* and axonal length at DIV7 was analyzed in GFP-expressing/TAU-stained Cgc (two-tailed unpaired t-test, $t(4) = 4.752$, (**) $P = 0.0090$, $n = 3$ from 3 litters). GFP-expressing cells also expressed hPKN1, as seen in overlapping GFP/HA-staining (image is representative of 3 separate experiments). Data is presented as individual *n*-values with mean±SEM. Cgc were grown on Laminin-coated coverslips and representative WIS-Neuromath-analyzed output-images are shown in **D** and **E**. All scale bars represent 50 μm. Experimenters were not blinded to the genotype or treatment.

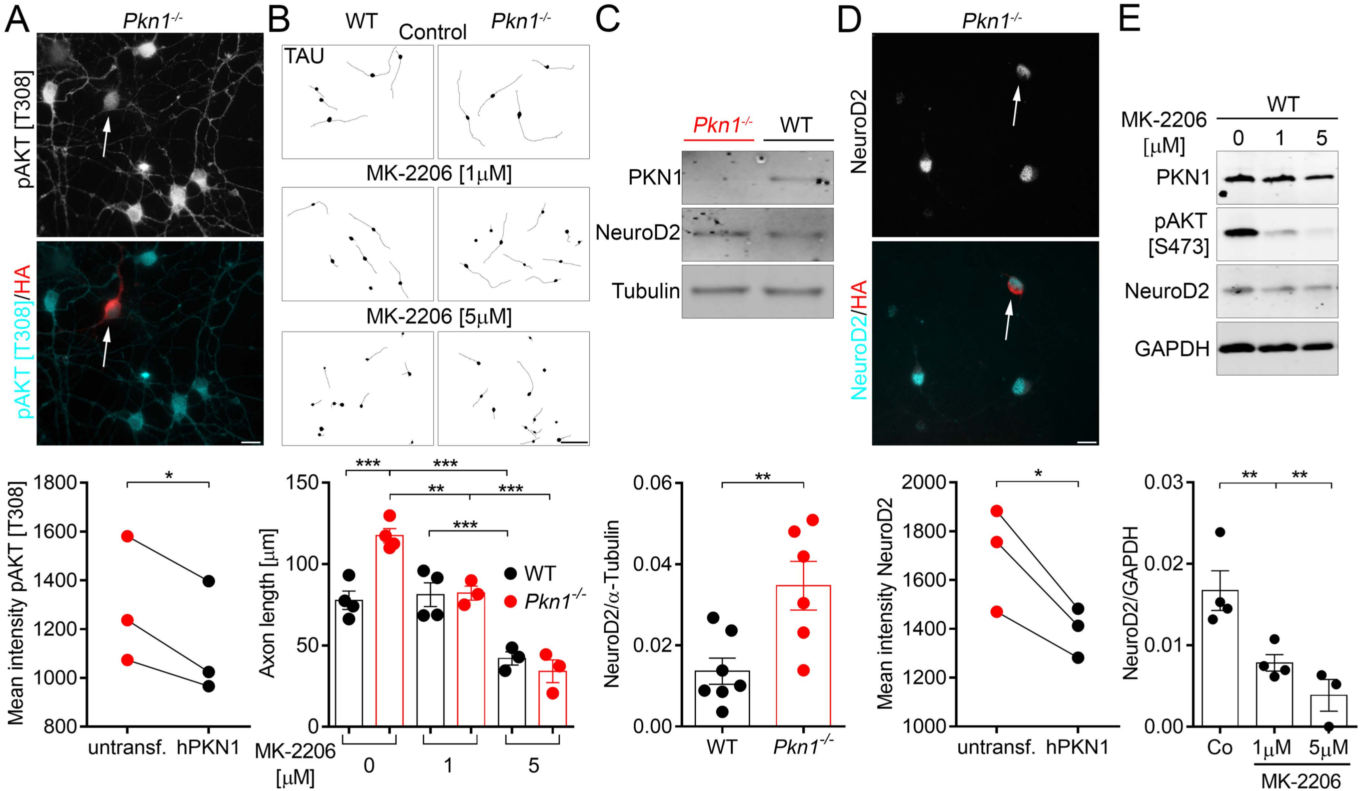

Figure 3. *Pkn1* knockout results in elevated AKT phosphorylation and NeuroD2 protein levels in Cgc in vitro. (**A**) phospho(p)-AKT [T308] intensity was measured in untransfected *Pkn1*$^{-/-}$ Cgc and *Pkn1*$^{-/-}$ Cgc expressing human HA-tagged (hPKN1) (8-22 transfected cells were analyzed/experiment, two-tailed paired t-test, $t(2) = 5.365$, (*) $P = 0.033$, $n = 3$ from 3 litters). (**B**) Cgc axonal length was measured at DIV1 after 24 h treatment with the AKT-inhibitor MK-2206 [1 or 5 μM] in TAU-stained Cgc (one-way ANOVA with Newman-Keuls multiple comparison test, $F(5,15) = 26.97$, $P < 0.0001$, post-test (**) $P < 0.01$, (***) $P < 0.001$, n = 3-4 WT/3-4 *Pkn1*$^{-/-}$ Cgc preparations from 3-4 litters/group). (**C**) NeuroD2 expression levels were analyzed in Cgc at DIV6-8 (two-tailed paired t-test, $t(11) = 3.228$, (**) $P = 0.008$, n = 7 WT/6 *Pkn1*$^{-/-}$ Cgc preparations from 6-7 different litters). Representative WIS-Neuromath-analyzed output-images are shown. (**D**) NeuroD2 intensity was measured at DIV4 in untransfected *Pkn1*$^{-/-}$ Cgc and *Pkn1*$^{-/-}$ Cgc expressing hPKN1 (26-32 transfected cells were analyzed/experiment, two-tailed paired t-test, $t(2) = 4.904$, (*) $P = 0.0392$, $n = 3$ from 3 litters). (**E**) WT Cgc protein extracts at DIV1 were analyzed for the effect of 24 h treatment of MK-2206 on NeuroD2 protein levels (one-way ANOVA with Newman-Keuls multiple comparison test, $F(2,8) = 11.76$, $P = 0.0042$, post-test (**) $P < 0.01$, n = 3-4 from 3-4 litters). All data is presented as individual n-values with mean±SEM. Scale bars in **A, D** represent 10 μm and in **B** 50 μm. Experimenters were not blinded to the genotype or treatment.

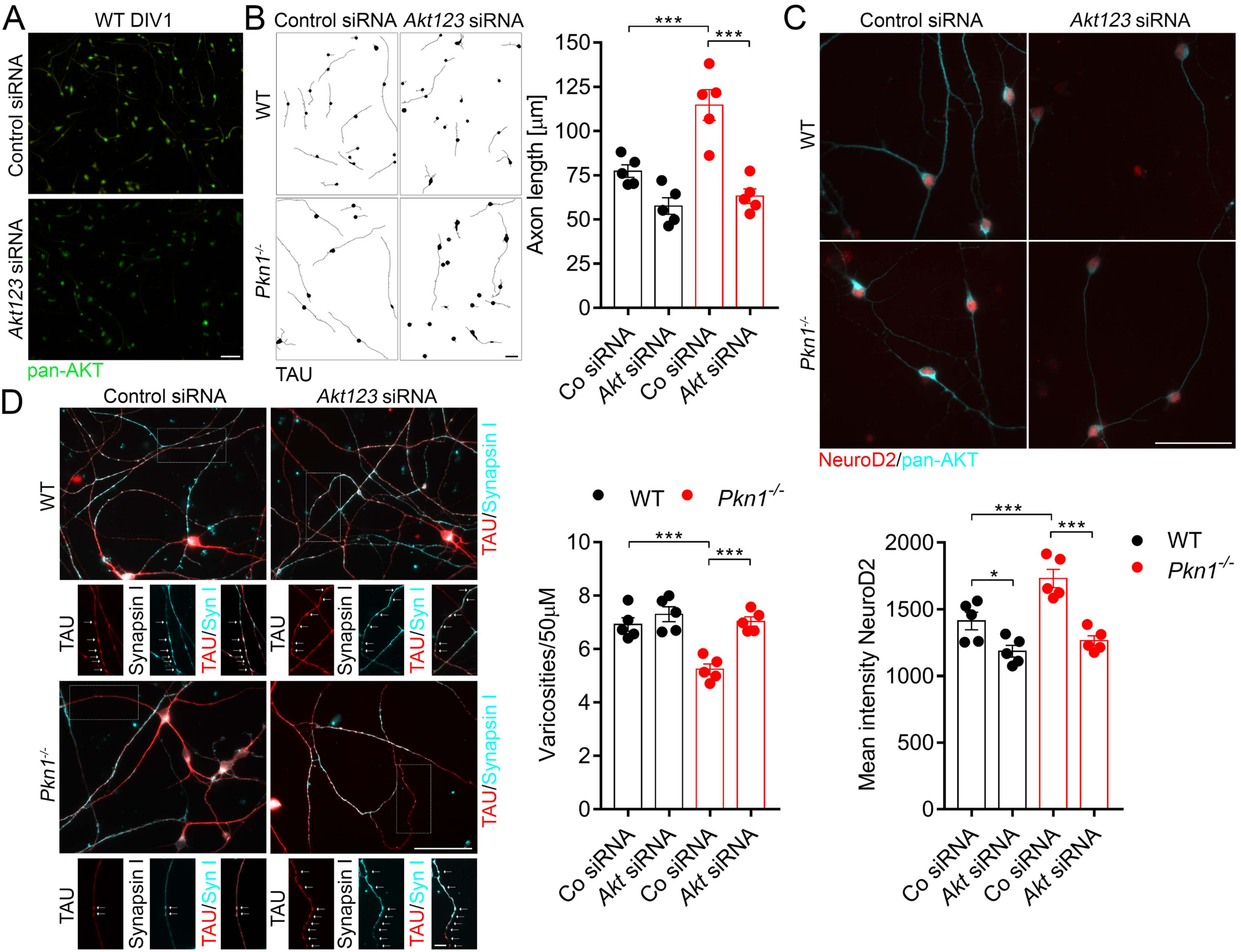

Figure 4. siRNA-mediated *Akt* knockdown reduces axonal length and NeuroD2 protein levels and increases the density of presynaptic sites in *Pkn1*$^{-/-}$ Cgc. (**A**) siRNAs targeting *Akt123* reduce pan-AKT expression after DIV1. Pictures are representative of 5 separate experiments. For analysis at DIV1 and DIV4 in WT and *Pkn1*$^{-/-}$ Cgc see Supplemental Figure 4, A and B. (**B**) siRNAs targeting *Akt123* significantly reduce axonal length of *Pkn1*$^{-/-}$ Cgc at DIV1 (one-way ANOVA with Newman-Keuls multiple comparison test, $F(3,16) = 20.78$, $P < 0.0001$, post-test (***) $P < 0.001$, $n = 5$ WT/5 *Pkn1*$^{-/-}$ Cgc preparations from 3-5 litters/group). Axons were stained with TAU. Representative WIS-Neuromath-analyzed output-images are shown. (**C**) siRNAs targeting *Akt123* significantly reduce NeuroD2 intensity in WT and *Pkn1*$^{-/-}$ Cgc at DIV4 (one-way ANOVA with Newman-Keuls multiple comparison test, $F(3,16) = 18.73$, $P < 0.0001$, post-test (*) $P < 0.05$, (***) $P < 0.001$, $n = 5$ WT/5 *Pkn1*$^{-/-}$ Cgc preparations from 3-5 litters/group). (**D**) Presynaptic sites (varicosities) were stained with TAU and Synapsin I. Insets represent higher magnification single- and double-labeled examples of axonal varicosities (indicated by arrows). White varicosities in double labeled insets demonstrate TAU and Synapsin I colocalization. siRNAs targeting *Akt123* significantly increase the density of presynaptic sites in *Pkn1*$^{-/-}$ Cgc at DIV4 (one-way ANOVA with Newman-Keuls multiple comparison test, $F(3,16) = 16.62$, $P < 0.0001$, post-test (***) $P < 0.001$, $n = 5$ WT/5 *Pkn1*$^{-/-}$ Cgc preparations from 3-5 litters/group). All data is presented as individual *n*-values with mean±SEM. All scale bars represent 50 µm, except for scale bar in inset in **D**, which represents 10 µm. Experimenters were not blinded to the genotype or treatment.

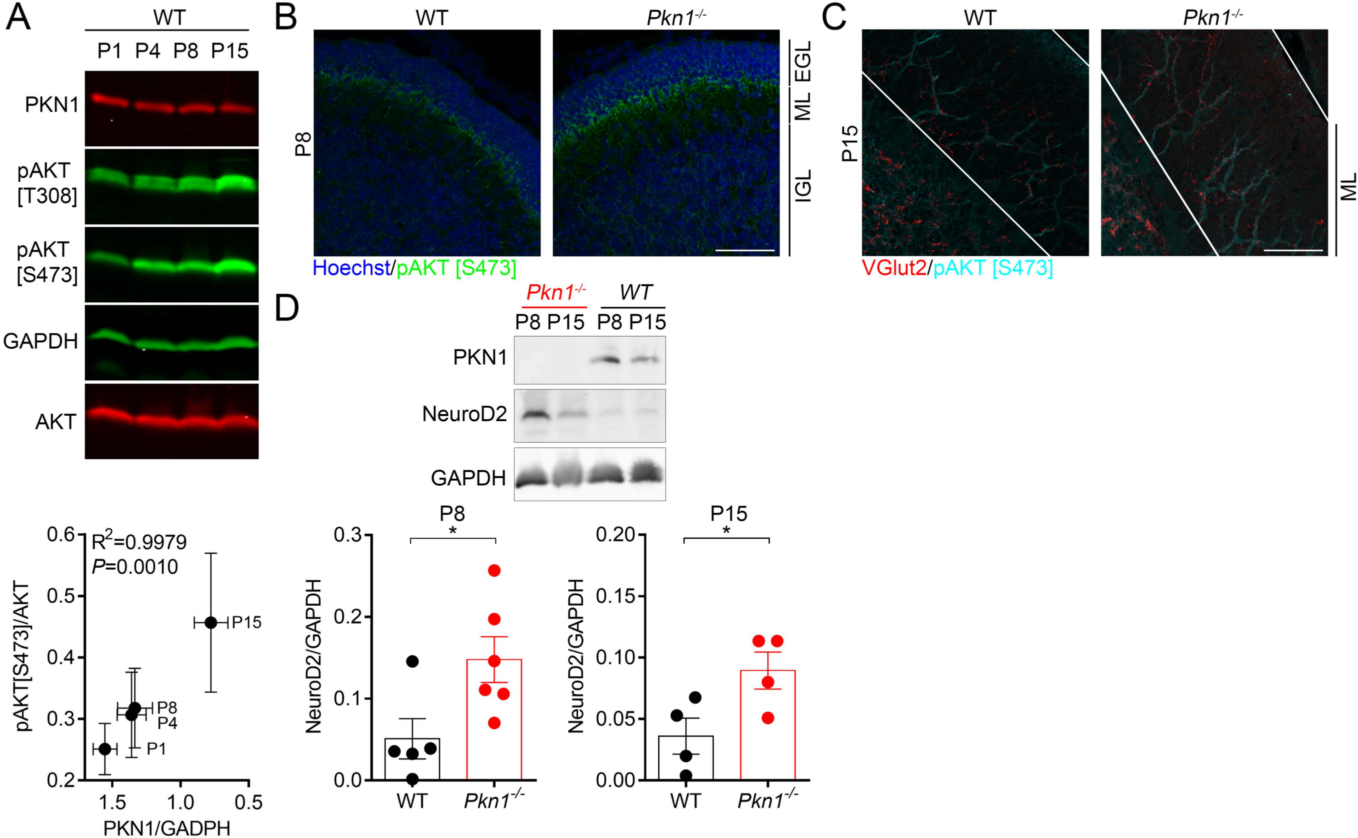

Figure 5. ***Pkn1*$^{-/-}$ cerebella show elevated AKT phosphorylation and NeuroD2 protein levels during developmental stages of parallel fiber maturation.** (**A**) There was a significant correlation between the pAKT [S473]/AKT ratio and the PKN1/GAPDH ratio in cerebellar protein extracts from P1-P15 old WT animals (Pearson correlation, Number of XY pairs: 4, Pearson r = -0.9990, (**, two-tailed) *P* = 0.001, R^2 = 0.9979, *n* = 3-4 from 3-4 litters/group). Data is presented as mean±SEM. (**B**) Confocal images of cerebellar sections of P8 and P15 old WT and *Pkn1*$^{-/-}$ animals stained for pAKT [S473] and Hoechst (P8) or (**C**) pAKT [S473] and VGlut2 (P15). Pictures are representative of at least 3 independent experiments. (**D**) Western blot analysis of NeuroD2 expression in P8 (two-tailed unpaired t-test, *t*(9) = 2.546, (*) *P* = 0.0314, *n* = 5 WT/6 *Pkn1*$^{-/-}$ animals from 4-5 different litters) and in P15 old WT and *Pkn1*$^{-/-}$ whole cerebella protein extracts (two-tailed unpaired t-test, *t*(6)=2.541, (*) *P* = 0.0440, *n* = 4 WT/4 *Pkn1*$^{-/-}$ animals from 4-5 different litters). Data is presented as individual *n*-values with mean±SEM. All scale bars represent 50 µm. Experimenters were not blinded to the genotype.

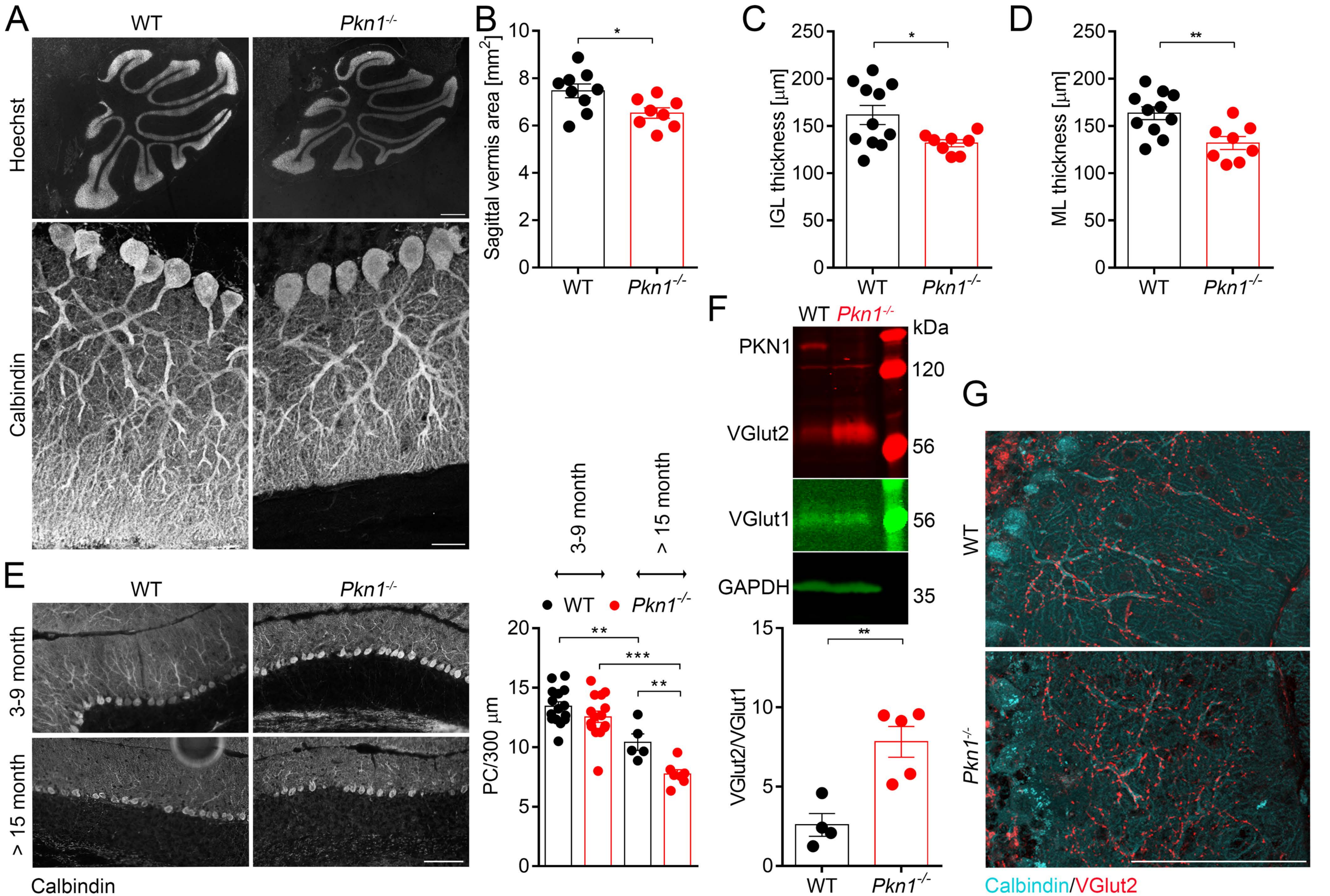

Figure 6. Adult $Pkn1^{-/-}$ mice show cerebellar shrinkage and late-onset Purkinje cell degeneration. (**A**) Size differences of adult WT and $Pkn1^{-/-}$ cerebella (3-9 month), as seen in Hoechst-stained sagittal vermis sections and Calbindin-stained ML pictures (representative images of 8-11 separate experiments, see Figure 6B-D for analysis). (**B**) Analysis of the cerebellar vermis area (two-tailed unpaired t-test, $t(15) = 2.510$, (*****) $P = 0.0236$, $n = 9$ WT/8 $Pkn1^{-/-}$ animals from 4-6 litters/group), (**C**) the thickness of the IGL (two-tailed unpaired t-test with Welch's correction, $t(12) = 2.772$, (*****) $P = 0.0169$, $n = 11$ WT/8 $Pkn1^{-/-}$ animals from 4-5 litters/group) and (**D**) the ML (two-tailed unpaired t-test, $t(17) = 3.210$, (******) $P = 0.0051$, $n = 11$ WT/8 $Pkn1^{-/-}$ animals from 4-5 litters/group) in 3-9 month old animals. (**E**) PC number in 3-9 month old and 15-22 month old animals (one-way ANOVA with Newman-Keuls multiple comparison test, $F(3,38) = 23.12$, $P < 0.0001$, post-test (******) $P < 0.01$, (*******) $P < 0.001$, $n = 5$-15 WT/7-15 $Pkn1^{-/-}$ animals). (**F**) Cerebellar protein extracts from 3-9 month old animals were analyzed for the VGlut2/VGlut1 ratio (two-tailed unpaired t-test, $t(7) = 4.138$, (******) $P = 0.0044$, $n = 4$ WT/5 $Pkn1^{-/-}$ animals from 4 litters/group). (**G**) Calbindin- and VGlut2-stained cerebellar sections of 3-9 month old animals (representative images of 11-12 experiments, see Supplemental Figure 6C for analysis). All data is presented as individual *n*-values with mean±SEM. Scale bars refer to **A** Hoechst 500 µm, Calbindin 50 µm, **E**/**G** 100 µm. All analyses were performed by experimenters blinded to the genotype, except for **F**.

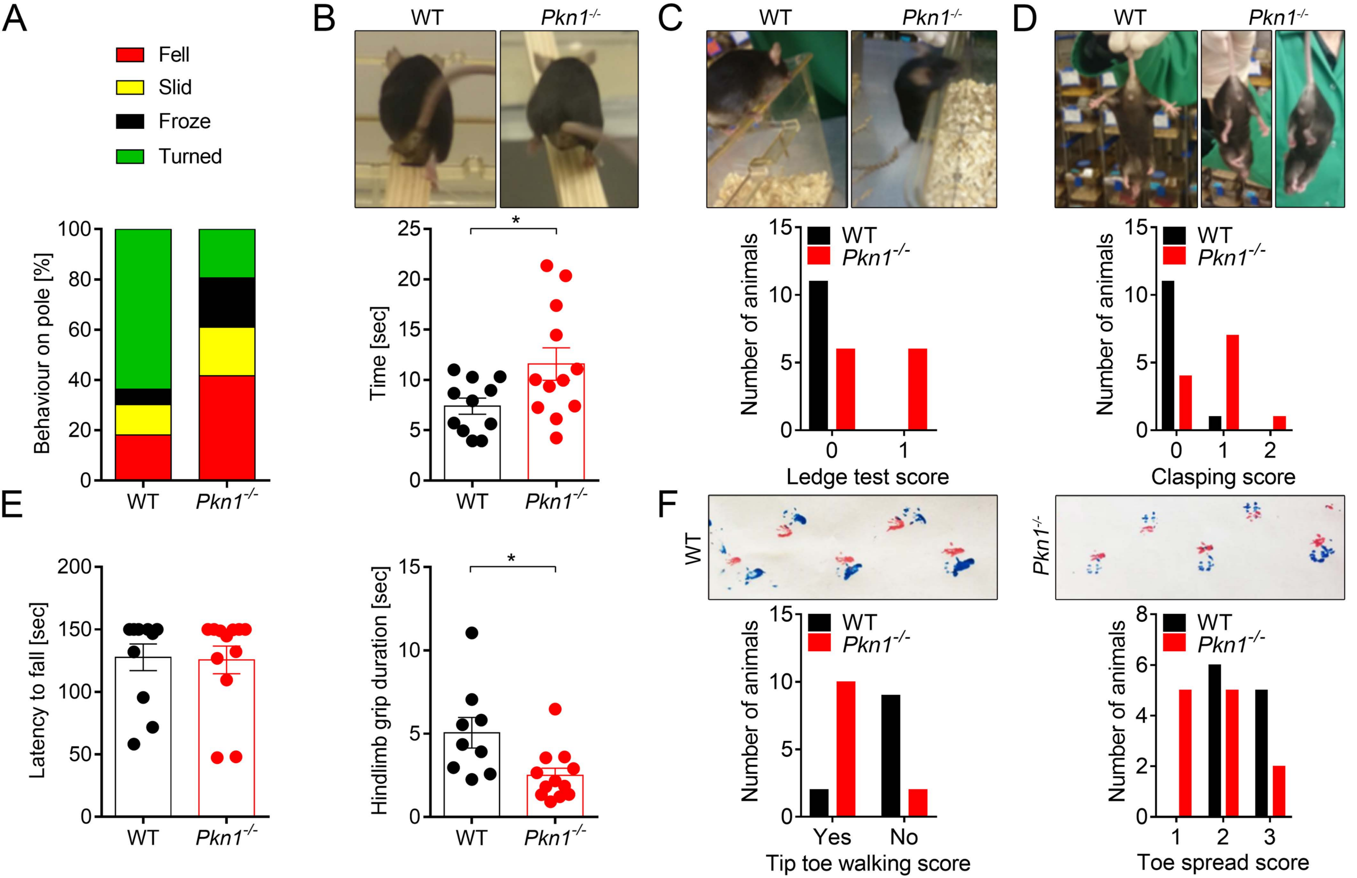

Figure 7. Adult *Pkn1*$^{-/-}$ animals have problems with balance and motor coordination. A cohort of adult (4-9 month) WT and *Pkn1*$^{-/-}$ animals was examined for motor deficits in a set of behavioral tests. (**A**) Adult mice were tested in the vertical pole-task (chi-square test (3) = 42.33, (***) $P < 0.0001$, n = 11 WT/12 *Pkn1*$^{-/-}$ animals from 4-6 litters/group). Data is presented as mean percentage. (**B**) Animals were tested in the balance beam test (two-tailed unpaired t-test with Welch's correction, $t(15) = 2.328$, (*) $P = 0.0334$, n = 11 WT/12 *Pkn1*$^{-/-}$ animals from 4-6 litters/group). (**C**) Animals were scored in the ledge test (chi-square test (1) = 7.441, (**) $P = 0.0064$, n = 11 WT/12 *Pkn1*$^{-/-}$ animals from 4-6 litters/group). (**D**) Animals were scored for hindlimb clasping (chi-square test (2) = 8.767, (*) $P = 0.0125$, n = 11 WT/12 *Pkn1*$^{-/-}$ animals from 4-6 litters/group). (**E**) In the wire hang test the grip strength, as determined by the latency to fall (two-tailed unpaired t-test, $t(21) = 0.1352$, $P = 0.8938$, n = 11 WT/12 *Pkn1*$^{-/-}$ animals from 4-6 litters/group) and hindlimb grip duration (two-tailed unpaired t-test, $t(19) = 2.724$, (*) $P = 0.0135$, n = 9 WT/12 *Pkn1*$^{-/-}$ animals from 4-6 litters/group) was assessed. (**F**) Footprints were scored for tip toe walking (chi-square test (1) = 9.763, (**) $P = 0.0018$, n = 11 WT/12 *Pkn1*$^{-/-}$ animals from 4-6 litters/group) and toe spread (chi-square test (2) = 6.345, (*) $P = 0.0419$, n = 11 WT/12 *Pkn1*$^{-/-}$ animals from 4-6 litters/group). Data in **B** and **E** is presented as individual n-values with mean±SEM. Experimenters were not blinded to the genotype, except for **F**.